Supporting Information

A Composite Surface Configuration towards Improving Cycling Stability of Li-Rich Layered Oxide Materials

Zhepu Shi,[a,b] Qingwen Gu,[a] Liang Yun,[a] Zhining Wei, [a,c] Di Hu,[b] Bao Qiu,[a] George Zheng Chen,*[d] and Zhaoping Liu*[a]*

[a]Ningbo Institute of Materials Technology and Engineering, Chinese Academy of Sciences (CAS), Ningbo, 315201, China

[b]Department of Chemical and Environmental Engineering, Faculty of Science and Engineering, The University of Nottingham, Ningbo, 315100, China

[c]School of Chemical Engineering and Technology, China University of Mining and Technology (CUMT), Xuzhou, 221166, China

[d]Department of Chemical and Environmental Engineering, Faculty of Engineering, The University of Nottingham, Nottingham, NG7 2RD, United Kingdom

[c]Corresponding author E-mail: qiubao@nimte.ac.cn (B. Qiu); george.chen@nottingham.ac.uk (G. Z. Chen); liuzp@nimte.ac.cn (Z. Liu)

Table S1. Results of the Rietveld analysis for P-LR-NCM and M-LR-NCM from FullProf. And related micro-strain analysis from JADE.

Sample	*a*/Å	*c*/Å	*c*/*a*	Li/Ni Mixing	R_{wp}/%	R_p/%	Strain (%)
P-LR-NCM	2.8503	14.240	4.9960	0.002	5.27	4.14	0.201(0.005)
M-LR-NCM	2.8514	14.241	4.9944	0.001	5.07	3.93	0.209(0.004)

Table S2. Materials and corresponding chemical analyses results.

Sample	Li	Ni	Co	Mn	Al	Nb
P-LR-NCM	1.380	0.172	0.171	0.656	0	0
M-LR-NCM	1.348	0.170	0.167	0.660	0.038	0.003

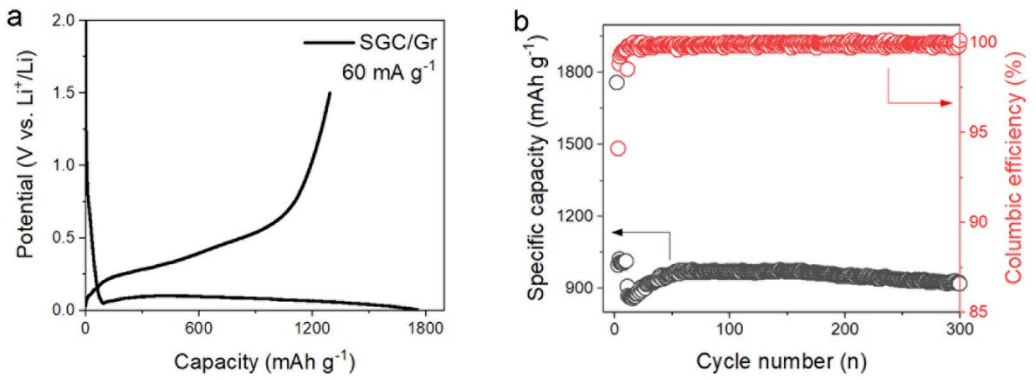

Figure S1. (a) The initial cycle profile of SGC/Gr at 0.05C, (b) the discharge capacity of SGC/Gr at 0.05C in subsequent 300 cycles.

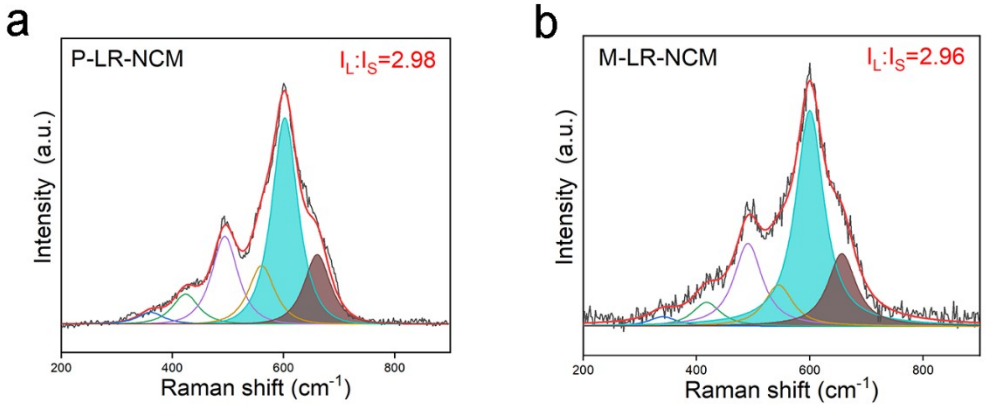

Figure S2. Raman spectra and the fitted results of P-LR-NCM and M-LR-NCM before cycling.

Figure S2 shows the two outstanding sharp peaks appeared at about 500 and 600 cm-1 are characteristic vibration modes of R-3m structure, implying the O-M-O bending (Eg) and M-O stretching (A1g) mode, respectively. The broaden peak existed at the range from 320 to 450 cm-1 reflects the remaining features of Li2MnO3 components. Exclusively, a weak and broad peak about 670 cm-1 for M-LR-NCM is attributed to the formation of spinel-like structure.

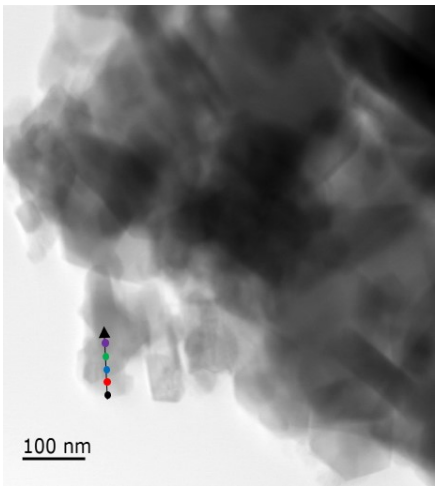

Figure S3. EELS line scan direction from surface (black dot) to bulk (purple dot) in the TEM image. The dots are corresponding to the different location of the scanning line.

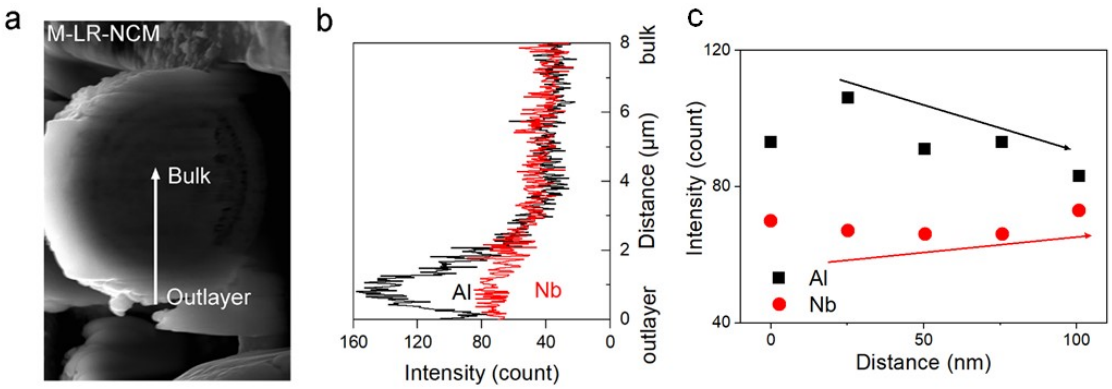

Figure S4. (a) a cross-section image of M-LR-NCM. Arrow indicates the direction of EDX line scan, (b) the corresponding EDX profile of Nb and Al from out layer to bulk along the direction in (a). (c) the enlarged near-surface region of (b).

Figure S4 shows an aggregated concentration of Nb and Al at the surface region from outlayer to 2 μm towards center. After this point, both of them gradually decrease and remain almost constant in the bulk region. At enlarged near-surface region, the gradually reduced intensity of Al indicates the elimination of Al_2O_3 coating and the appearance of doping region once reaching 25 nm.

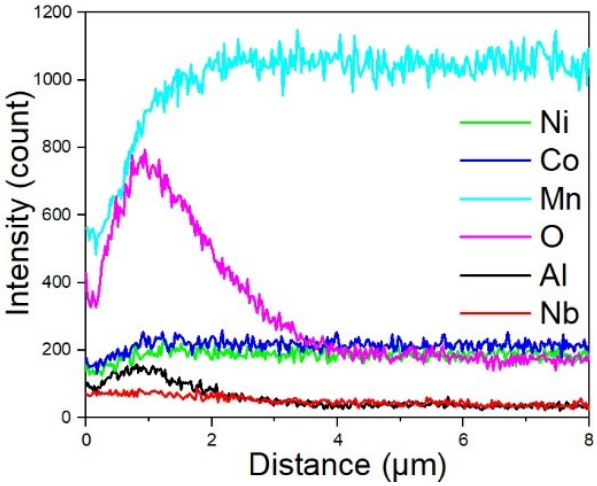

Figure S5. EDX line scan of cross-section M-LR-NCM sample. All elements are involved.

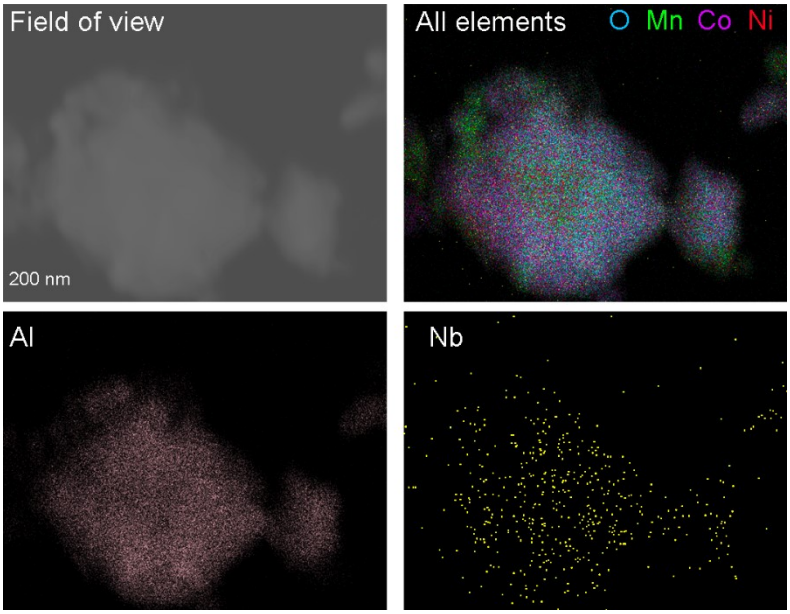

Figure S6. The corresponding EDS mapping of M-LR-NCM from TEM.

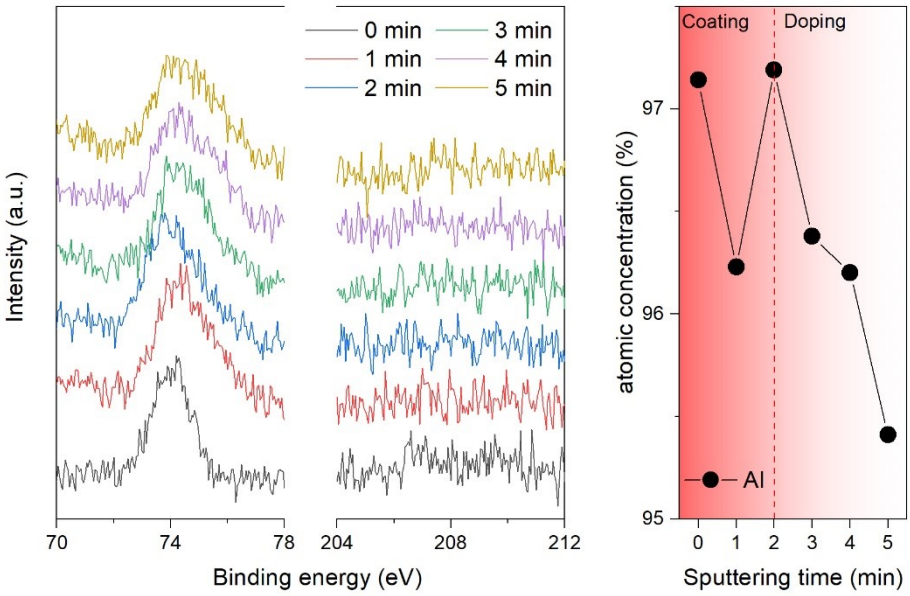

Figure S7. (a) The XPS spectra of Al and Nb during Ar^+ etching of M-LR-NCM, (b) the variation of corresponding atomic concentration versus the sputtering time based on the comparison between Al and Nb elements.

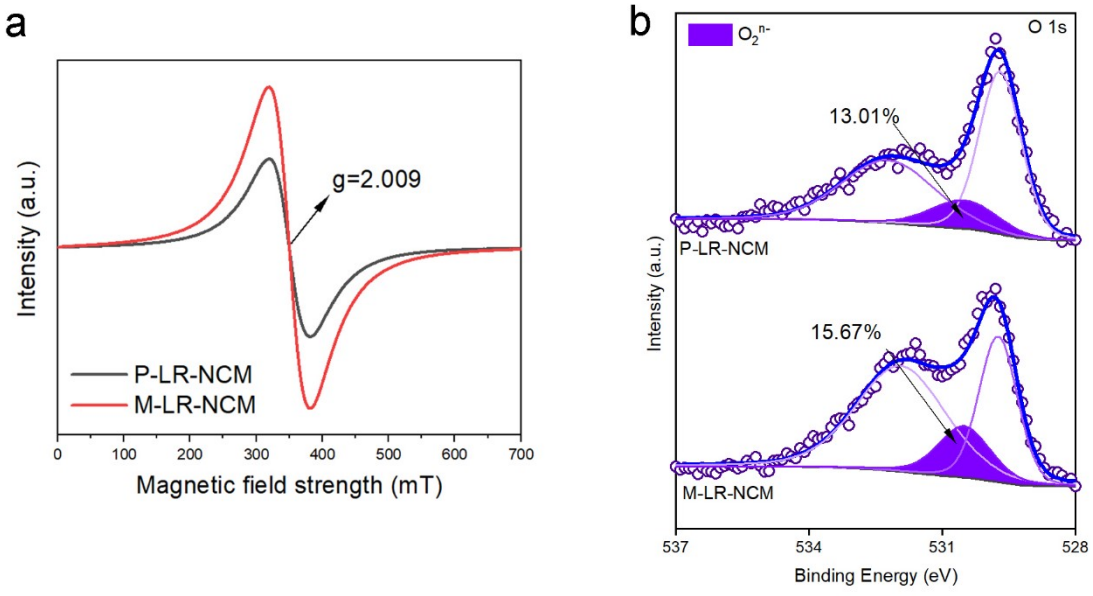

Figure S8. (a) The EPR spectra of both samples, (b) the O 1s fitting results with respective amounts of oxygen vacancies in P-LR-NCM and M-LR-NCM.

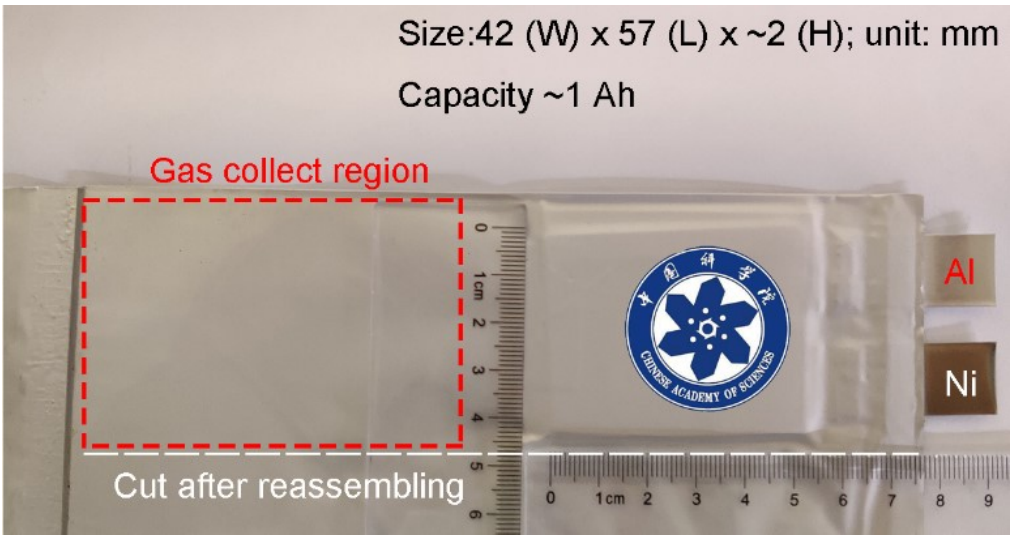

Figure S9. Illustration of home-made ~1 Ah pouch cell designed for GC measurement.

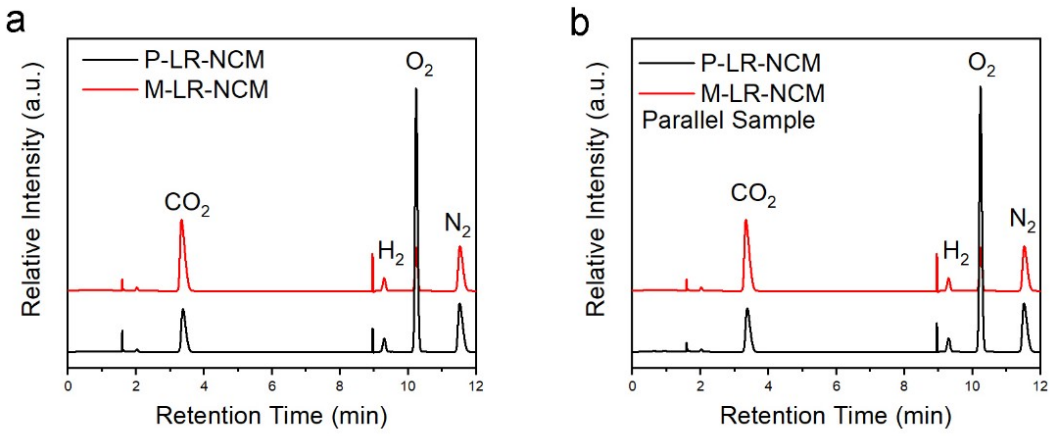

Figure S10. GC profile of gas components collected from the pouch cells after first cycle. (b) Parallel experiments used to verify the results from (a).

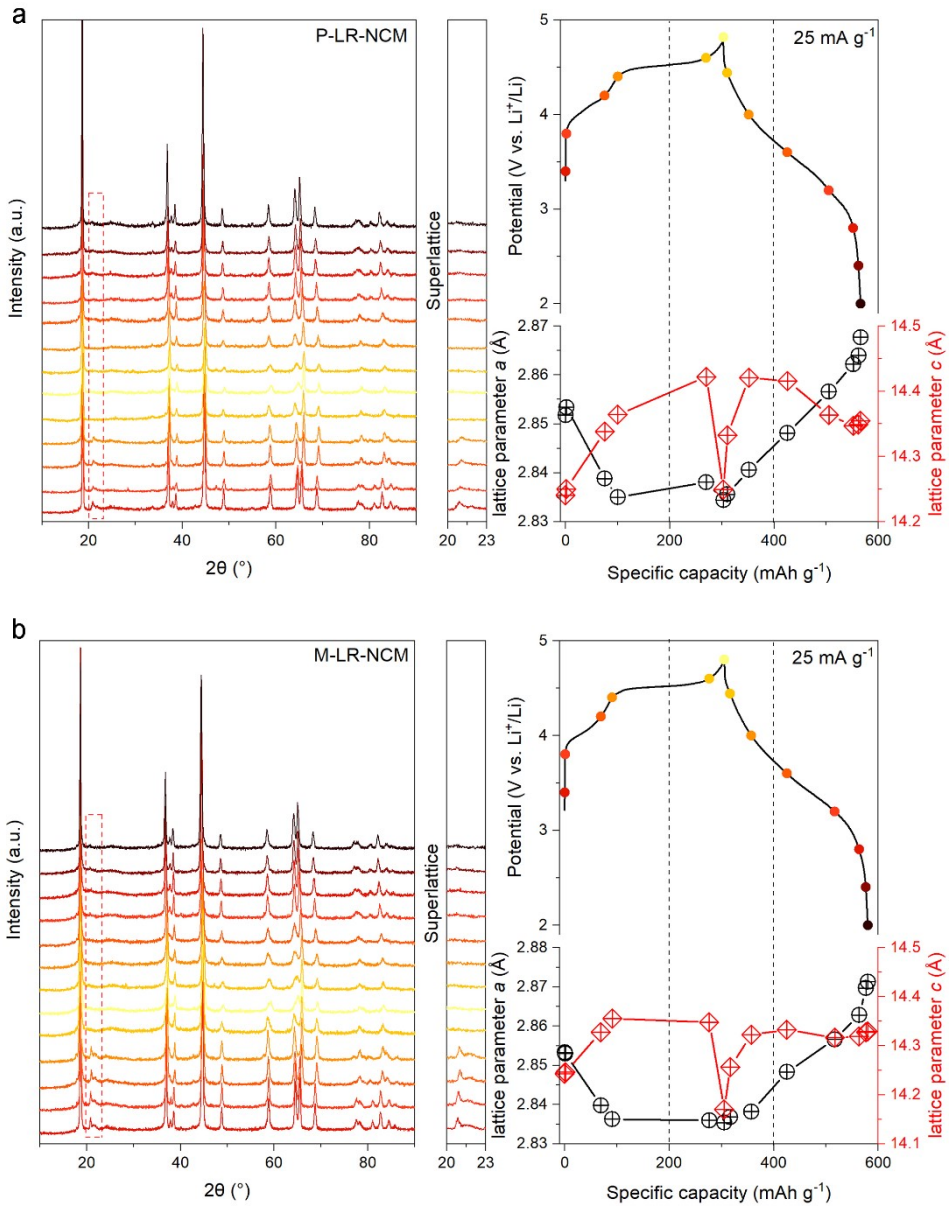

Figure S11. *Ex-situ* XRD results with corresponding lattice parameters of (a) P-LR-NCM and (b) M-LR-NCM at various potential (from left to right, 3.4V, 3.8V, 4.2V, 4.4V, 4.6V, 4.8V at charging; 4.4V, 4.0V, 3.6V, 3.2V, 2.8V, 2.4V, 2.0V at discharging) during first cycle.

As shown in **Figure S11**, the structural evolutions of two samples during first cycle were exhibits. The superlattice structures of both samples were disappeared at 4.6 V, indicating the deintercalation of Li ions from the Li_2MnO_3 domains and activation of O redox. After discharging to 3.2 V, a relatively weak peak reappeared at the position of superlattice structures, which was caused by the intercalated Li ions back to TM layer. However, since the in-plane TM migration disturbed the original arrangement of TM layer,[1] the intensity of superlattice structures was significantly reduced as compared to non-activated one. The similar evolution of superlattice structures illustrated the composite surface configuration would not interrupt the O redox though it exerted positive effects on mitigating gas release. As for the whole structural evolution during first cycle, the corresponding evolution of lattice parameter *a* and *c* suggested a similar behavior

for both samples except the restricted *c* evolution of M-LR-NCM. As for the *c* expansion, P-LR-NCM underwent 0.80 % expansion, while that was 0.61% for M-LR-NCM. The severer expansion of *c* demonstrated the lattice distortion of the host framework.[2] Once it came to the entire volume, P-LR-NCM expanded from 100.305 to 102.233, the lattice expansion was 1.92 %. However, M-LR-NCM only expanded 1.88 % after first cycle. The gas release at first cycle greatly accelerated the structural rearrangement around surface, which further enforced the lattice distortion as the partial frame oxygen ions were lost. The mitigated structural expansion at first cycle revealed the enhanced structural stability of M-LR-NCM due to reduced oxygen evolution.

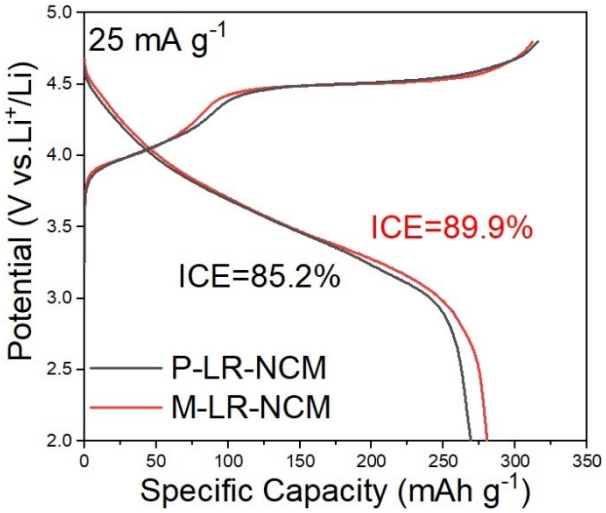

Figure S12. The initial charge-discharge profile of P-LR-NCM and M-LR-NCM at 25 mA g^{-1} between 2.0 to 4.8 V.

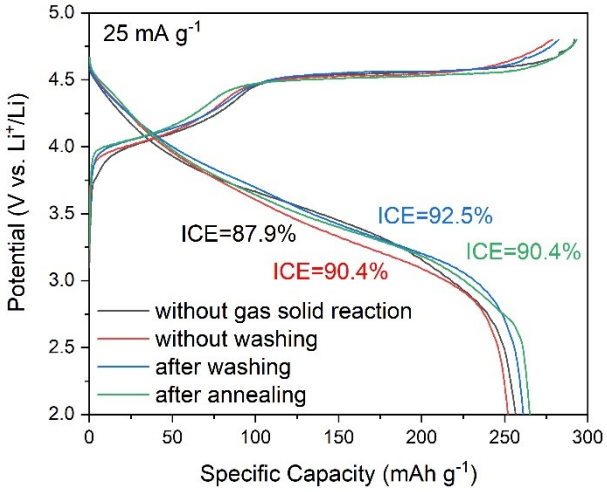

Figure S13. The initial charge-discharge profile of M-LR-NCM with different conditions at 25 mA g^{-1} between 2.0 to 4.8 V.

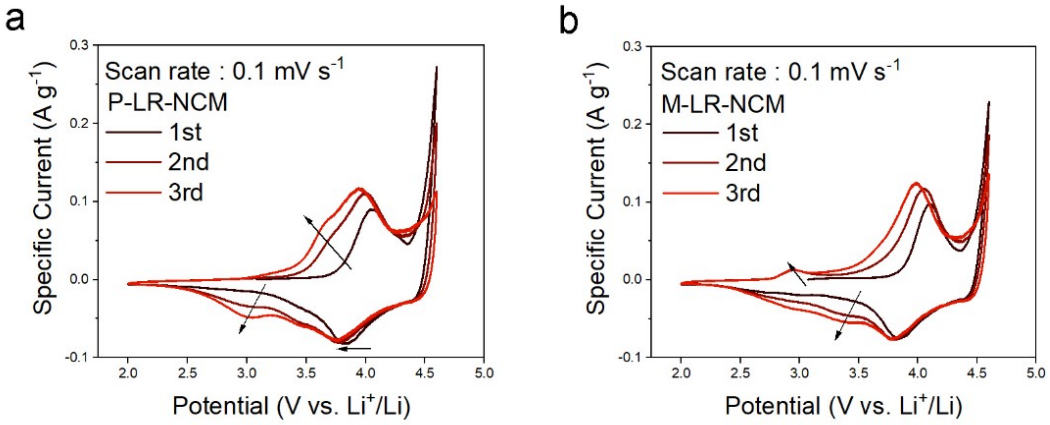

Figure S14. CVs for the initial three cycles of (a) P-LR-NCM and (b) M-LR-NCM at 0.1 mV s^{-1} scan rate.

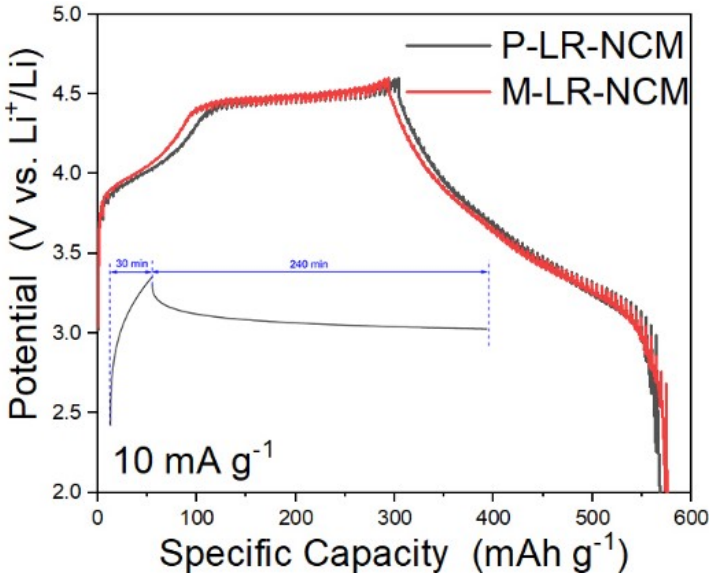

Figure S15. GITT results of P-LR-NCM and M-LR-NCM during first cycle. The inset is a schematic illustration of a single step of the GITT with the interval 30 min charge or discharge at a specific current of 10 mA g^{-1} and 240 min relaxation.

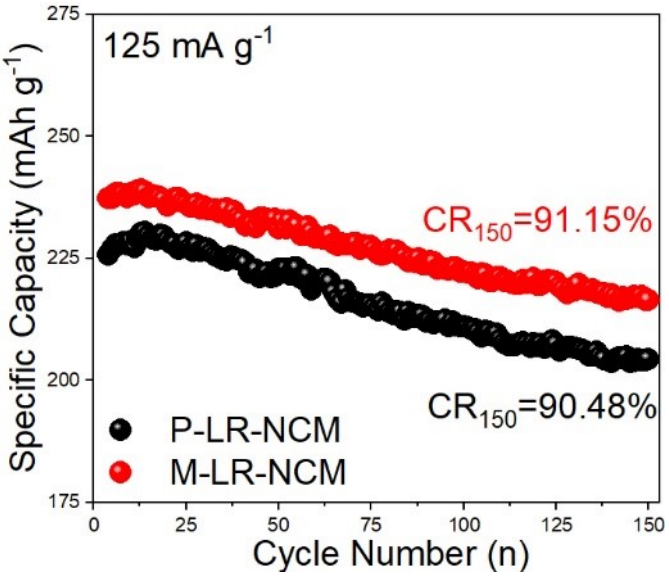

Figure S16. The cycling performance of P-LR-NCM and M-LR-NCM at 125 mA g^{-1}.

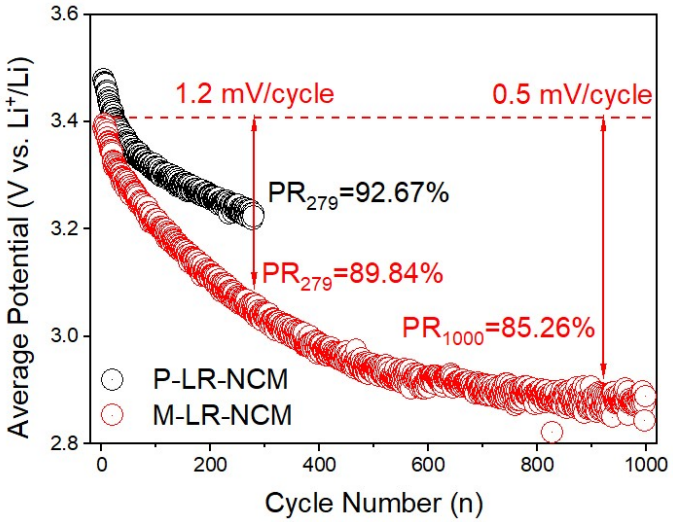

Figure S17. The potential decay of P-LR-NCM and M-LR-NCM at 250 mA g^{-1}.

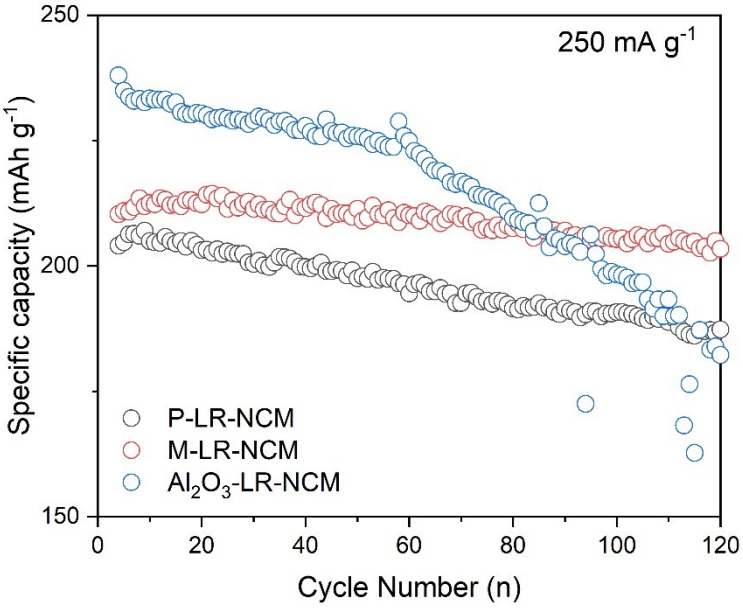

Figure S18. The specific discharging capacity of P-LR-NCM, M-LR-NCM and Al_2O_3-LR-NCM (Al_2O_3 coated P-LR-NCM) at 250 mA g^{-1} during 120 cycles.

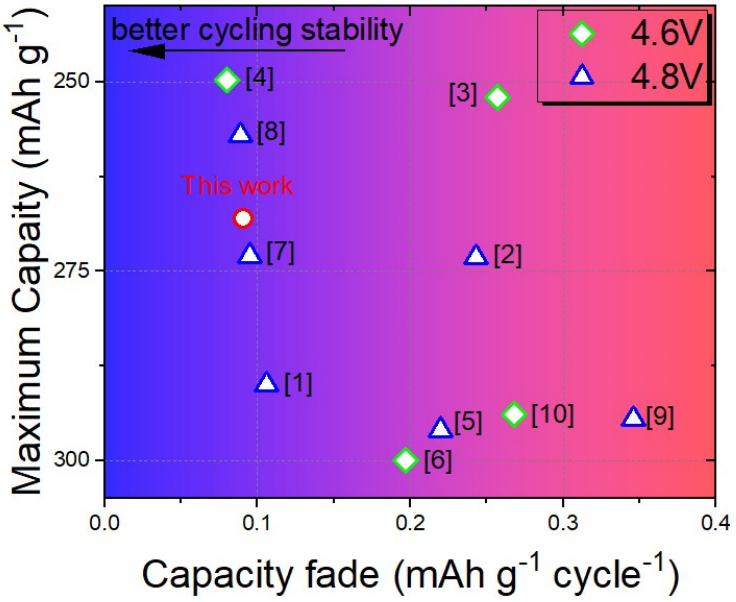

Figure S19. Electrochemical performance comparisons with other mainstream reports.

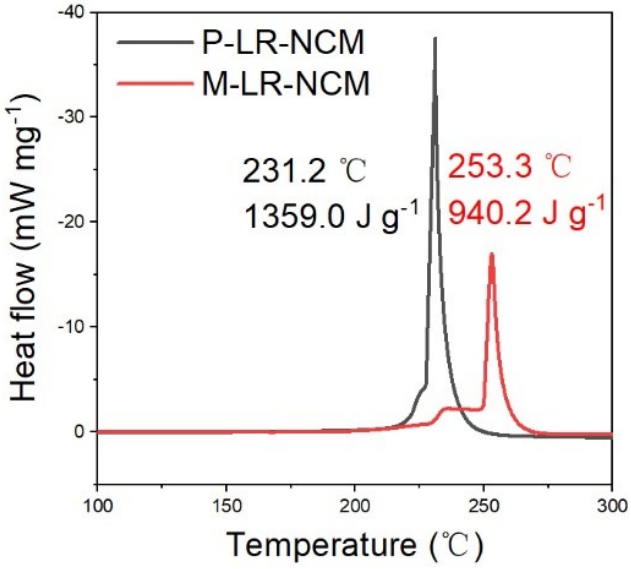

Figure S20. DSC results of P-LR-NCM and M-LR-NCM after charging to 4.8V.

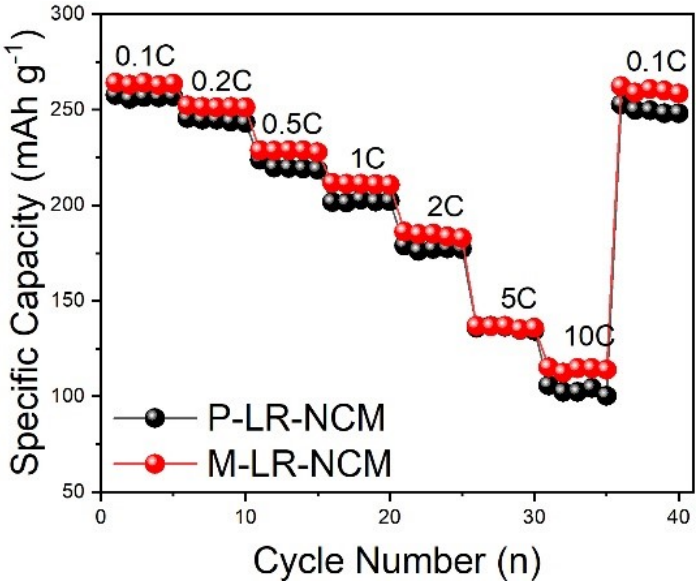

Figure S21. The rate performance of P-LR-NCM and M-LR-NCM at room temperature.

Table S3. Summarized electrochemical performances of advanced LR-NCM materials from mainstream reports. The symbol ~ indicates estimated values from figures of each reference.

Modification	Capacity Maximum	Cycling Performances			Test conditions
	@RT (mAh g^{-1})	Specific capacity (mAh g^{-1})	Capacity retention	Average Capacity fade (mAh g^{-1} $cycle^{-1}$)	Specific current (mA g^{-1})
Ref[1]-Spinel $LiCoO_2$[3]	290 (12.5 mA g^{-1} 4.8V)	205	79.3% at 400th	0.106	250
Ref[2]-$LiTaO_3$ ALD coating[4]	273.2 (20 mA g^{-1} 4.8V)	~220	78% at 200th	0.243	200
Ref[3]-Ammonia treatment @400 ^oC[5]	252 (25 mA g^{-1})	226	93.3% at 60th	0.257	83.3
Ref[4]-H_2SO_4 treatment[6]	249.7 (25 mA g^{-1})	196.5	79.8% at 500th	0.080	250
Ref[5]-oleic acid[7]	296 (25 mA g^{-1} 4.8V)	277	84.1% at 200th	0.220	250
Ref[6]-$NH_3 \cdot H_20$[8]	300 (20 mA g^{-1})	~261	85% at 200th	0.197	100
Ref[7]-$NiFe_2O_4$[9]	273 (26mA g^{-1} 4.8V)	232.5	91.8% at 200th	0.095	260
Ref[8]- Ni-rich surface[10]	257.1 (25 mA g^{-1} 4.8V)	232	92.3% at 200th	0.089	250
Ref[9]-Yb doping[11]	294.5 (26 mA g^{-1} 4.8V)	219.8	84.4% at 100th	0.346	250
Ref[10]-B doping[12]	293.9 (10 mA g^{-1})	255.4	89.5% at 100th	0.268	100
This work	268.1 (25 mA g^{-1})	210.3	57.0% at 1000th	0.091	250

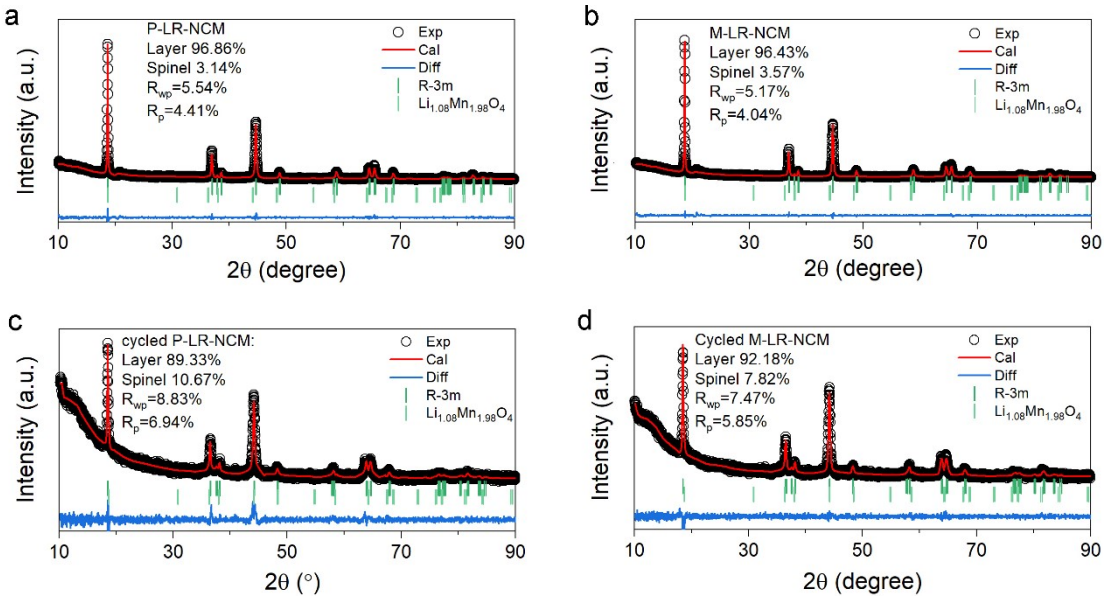

Figure S22. Rietveld refinement XRD through FullProf via double phase models. (R-3m and Fd-3m). (a)P-LR-NCM, (b) M-LR-NCM, (c) cycled P-LR-NCM and (d) cycled M-LR-NCM.

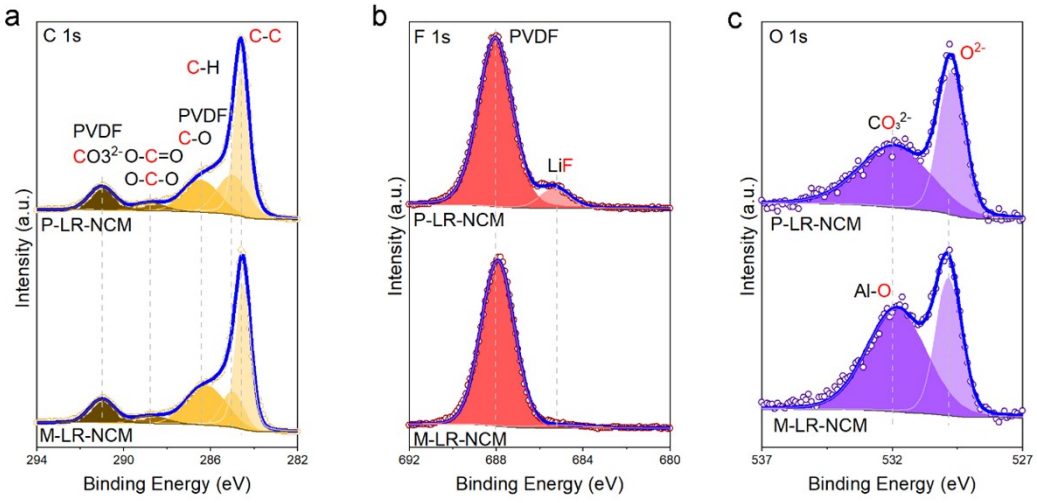

Figure S23. Comparison of XPS spectra of (a) C 1s, (b) F 1s and (c) O 1s of P-LR-NCM and M-LR-NCM before cycling.

Table S4. Results of the Rietveld analysis for P-LR-NCM and M-LR-NCM after 200 cycle at 1C from FullProf. And related micro-strain analysis from JADE.

Sample	*a*/Å	*c*/Å	Li/Ni Mixing	R_{wp}/%	R_p/%	Strain(%)
P-LR-NCM	2.8890	14.424	0.006	5.50	6.98	0.471(0.0108)
M-LR-NCM	2.8810	14.370	0.005	5.48	6.97	0.362(0.0097)

References

1. R. A. House, J.-J. Marie, M. A. Pérez-Osorio, G. J. Rees, E. Boivin and P. G. Bruce, *Nat. Energy*, 2021, **6**, 781-789.
2. X. D. Zhang, J. L. Shi, J. Y. Liang, Y. X. Yin, J. N. Zhang, X. Q. Yu and Y. G. Guo, *Adv. Mater.*, 2018, **30**, 1801751.
3. Y. Liu, H. Zhu, H. Zhu, Y. Ren, Y. Zhu, Y. Huang, L. Dai, S. Dou, J. Xu, C. J. Sun, X. L. Wang, Y. Deng, Q. Yuan, X. Liu, J. Wu, Y. Chen and Q. Liu, *Adv. Energy Mater.*, 2021, **11**, 2003479.
4. E. Wang, Y. Zhao, D. Xiao, X. Zhang, T. Wu, B. Wang, M. Zubair, Y. Li, X. Sun and H. Yu, *Adv. Mater.*, 2020, **32**, 1906070.
5. E. M. Erickson, H. Sclar, F. Schipper, J. Liu, R. Tian, C. Ghanty, L. Burstein, N. Leifer, J. Grinblat, M. Talianker, J.-Y. Shin, J. K. Lampert, B. Markovsky, A. I. Frenkel and D. Aurbach, *Adv. Energy Mater.*, 2017, **7**, 1700708.
6. H. C. Guo, Z. Wei, K. Jia, B. Qiu, C. Yin, F. Q. Meng, Q. H. Zhang, L. Gu, S. J. Han, Y. Liu, H. Zhao, W. Jiang, H. F. Cui, Y. G. Xia and Z. P. Liu, *Energy Storage Mater.*, 2019, **16**, 220-227.
7. W. Guo, C. Zhang, Y. Zhang, L. Lin, W. He, Q. Xie, B. Sa, L. Wang and D. L. Peng, *Adv. Mater.*, 2021, **33**, 2103173.
8. B. Wu, X. Yang, X. Jiang, Y. Zhang, H. Shu, P. Gao, L. Liu and X. Wang, *Adv. Funct. Mater.*, 2018, **28**, 1803392.
9. J. Peng, Y. Li, Z. Chen, G. Liang, S. Hu, T. Zhou, F. Zheng, Q. Pan, H. Wang, Q. Li, J. Liu and Z. Guo, *ACS Nano*, 2021, 15, 11607-11618.
10. H. Zheng, Z. Hu, P. Liu, W. Xu, Q. Xie, W. He, Q. Luo, L. Wang, D. Gu, B. Qu, Z.-Z. Zhu and D.-L. Peng, *Energy Storage Mater.*, 2020, **25**, 76-85.
11. L. Bao, Z. Yang, L. Chen, Y. Su, Y. Lu, W. Li, F. Yuan, J. Dong, Y. Fang, Z. Ji, C. Shi and W. Feng, *ChemSusChem*, 2019, **12**, 2294-2301.
12. Z. H. Sun, L. Q. Xu, C. Q. Dong, H. T. Zhang, M. T. Zhang, Y. Y. Liu, Y. Zhou, Y. Han and Y. S. Chen, *J. Mater. Chem. A*, 2019, **7**, 3375-3383.